

Energy gap opening in submonolayer lithium on graphene: Local density functional and tight-binding calculations

M. Farjam¹ and H. Rafii-Tabar^{1,2}

¹*Department of Nano-Science, Computational Physical Sciences Laboratory, Institute for Research in Fundamental Sciences (IPM), P.O. Box 19395-5531, Tehran, Iran*

²*Department of Medical Physics and Biomedical Engineering, and Research Centre for Medical Nanotechnology and Tissue Engineering, Shahid Beheshti University of Medical Sciences, Evin, Tehran 19839, Iran*

(Dated: June 18, 2021)

The adsorption of an alkali-metal submonolayer on graphene occupying every third hexagon of the honeycomb lattice in a commensurate $(\sqrt{3} \times \sqrt{3})R30^\circ$ arrangement induces an energy gap in the spectrum of graphene. To exemplify this type of band gap, we present *ab initio* density functional theory calculations of the electronic band structure of C_6Li . An examination of the lattice geometry of the compound system shows the possibility that the nearest-neighbor hopping amplitudes have alternating values constructed in a Kekulé-type structure. The band structure of the textured tight-binding model is calculated and shown to reproduce the expected band gap as well as other characteristic degeneracy removals in the spectrum of graphene induced by lithium adsorption. More generally we also deduce the possibility of energy gap opening in periodic metal on graphene compounds C_xM if x is a multiple of 3.

PACS numbers: 73.22.-f, 73.20.At, 81.05.Uw

I. INTRODUCTION

The isolation of graphene, a honeycomb lattice of carbon atoms, and the observation of the electric-field effect in the nanostructured samples, deposited on oxidized silicon surface, have renewed interest in the electronic properties of this two-dimensional carbon material.¹ The breakthrough discovery made possible the experimental observation of theoretically predicted exotic physics of graphene, including an anomalous half-integer quantum Hall effect, non-zero Berry's phase, and minimum conductivity.^{2,3}

The exceptional properties of graphene, two-dimensional structure and room-temperature high mobility, make it an ideal material for carbon-based nanoelectronics envisaged in the future nanotechnologies. Various applications depend on the possibility of fabricating a graphene-based field effect transistor (FET), including transistors to be used in nanoscale electronic circuits, light emitters and detectors, and ultra-sensitive chemical sensors and biosensors.⁴ Being a zero-gap semiconductor, however, graphene cannot be used directly as the conducting channel in FETs. Discovering how to generate band gaps is therefore a question of fundamental and applied significance. Several possibilities exist. Lateral confinement of the charge carriers in graphene nanoribbons (GNRs),⁵ and different gate voltages applied to the two layers of bilayer graphene are promising methods of engineering band gaps in graphene.⁶ Recently, a band gap has been discovered in epitaxial graphene derived from graphitization of silicon carbide.⁷ The effect of a substrate-induced band gap has also been investigated experimentally in epitaxial graphene on nickel,⁸ and theoretically in graphene on boron nitride.⁹

One of the routes toward tailoring the electronic properties of graphene is through the adsorption of metals.^{10,11} Alkali metals, in particular, are donors of electrons and can be used for the purpose of doping graphene to change its carrier concentration. The related problem of adsorption of alkali metals on graphite, which consists of weakly linked layers of graphene, has been studied extensively in the past.¹² In a quite recent study, a band gap was experimentally observed, and theoretically confirmed, in the surface electronic structure of graphite, induced by the adsorption of sodium in a (5×5) model.¹³ The similar effect has also been reported for the (4×4) model.¹⁴ Due to the heavy doping, however, the Fermi level is displaced into the graphene conduction π^* band so that the band gap lies in the occupied levels. The gap-inducing mechanism in these cases involves doping as well as interaction between the graphene layers in the graphite surface.

In this paper, we study the gap-inducing effect of alkali-metal adsorption on single layer graphene, which represents a different problem than graphite surface since the gap cannot be due to interlayer interactions. For instance, first-principles calculations of metal adsorption on graphene in the (4×4) model¹⁵ do not show a gap at the Dirac point in the density of states (DOS). We present the case of lithium on graphene compound C_6Li in detail for several reasons. This is a prototypical system in which the gap opening effect occurs, it is a simple system to study theoretically, and it may be accessible experimentally. The crucial property here is the structure of the system, so that other alkali and alkaline-earth metal compounds C_6M can exhibit the same effect. For instance, a similar band gap has been calculated for calcium graphite intercalated compound,¹⁶ as well as for calcium on graphene, both as C_6Ca .¹⁷ Due to doping,

lithium or another alkali metal on graphene results in a metal and is not directly useful for semiconductor applications. It is, however, important to understand the mechanism responsible for the gap opening effect.

An interesting question is which coverages of an alkali metal on graphene can induce a band gap in its spectrum. Our first-principles density functional theory (DFT) calculations indicate the absence of a gap in (1×1) , (2×2) , and (4×4) models, corresponding to C_2Li , C_8Li , and $C_{32}Li$, respectively, but its presence in the $(\sqrt{3} \times \sqrt{3})R30^\circ$ structure, which includes C_3Li and C_6Li , as well as in (3×3) coverage $C_{18}Li$. Explaining the underlying reason is the subject of the following sections.

Our paper is organized as follows. Section II presents the results of DFT calculations. Section III develops the tight-binding (TB) model. It includes a description of the lattice geometry, from which we clarify the gap mechanism within the TB model. We conclude here that, when lithium atoms are arranged above the hollow sites of graphene honeycomb lattice in a periodic commensurate structure to form C_6Li , the nearest-neighbor hopping amplitudes acquire alternating values constructed in a Kekulé-type structure. This section also includes a discussion of the TB Hamiltonian and numerical results for the Kekulé textured model with two hopping amplitudes. Section IV contains a summary and conclusion. The Appendix develops the solution of the TB model.

II. DFT CALCULATIONS

Quantitative data for the electronic band structure of C_6Li were obtained from DFT calculations, using a plane wave basis set and pseudopotentials. We used the QUANTUM-ESPRESSO code and norm-conserving pseudopotentials,¹⁸ and performed the calculations with local-density approximation (LDA) and Perdew-Zunger parametrization¹⁹ of the Ceperley-Alder correlation functional.²⁰ We used a lattice parameter of $a_0 = 2.46 \text{ \AA}$ for graphene, corresponding to a C-C bond length of 1.42 \AA . Other theoretical calculations¹⁵ have shown that alkali metals generally prefer to adsorb on the hollow sites of graphene rather than the bridge or top sites. We positioned the lithium atoms over the hollow sites of graphene in a $(\sqrt{3} \times \sqrt{3})R30^\circ$ commensurate superstructure. We remark, however, that lithium has not been shown to coat graphene or graphite in this manner.¹² As a first approximation and in view of the strength of the graphene bonds, initially we used the DFT code to only relax the distance of lithium atoms from the graphene plane, keeping the coordinates of carbon atoms fixed. This yielded a distance of 1.79 \AA between the lithium layer and graphene, which is a somewhat smaller value, as expected for the LDA, than that obtained in other theoretical calculations based on generalized-gradient approximation (GGA).¹⁴ In our tight-binding model presented in the Sec. III we use the data obtained for this structure. However, since a change

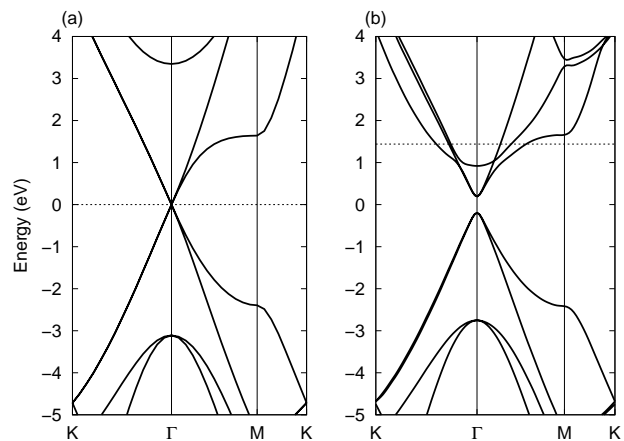


FIG. 1: (a) Band structure of C_6^* , i.e., graphene described by the unit cell of $(\sqrt{3} \times \sqrt{3})R30^\circ$ structure. (b) Band structure of C_6Li . A band gap has opened at the neutrality point, the degenerate bands along the Γ - K direction are split, and a small band gap has opened at K near the bottom of the figure. Horizontal dashed lines indicate the Fermi levels of the respective systems.

in the bond lengths has an important implication for opening a band gap, we then used the code to relax the positions of the carbon atoms as well as the position of lithium atoms. This indeed resulted in a tiny Kekulé distortion of C-C bond lengths, so that the near bonds to Li were contracted by $2.8 \times 10^{-4} \text{ \AA}$, and the far bonds to Li were stretched by $5.6 \times 10^{-4} \text{ \AA}$. We then made band structure and DOS calculations for C_6Li . For repeated images of the systems, we used supercells, with $c = 12 \text{ \AA}$ for graphene, and $c = 15 \text{ \AA}$ for C_6Li . A kinetic-energy cutoff of 70 Ry was needed for total-energy convergence. Brillouin-zone (BZ) integrations were made with a $6 \times 6 \times 2$ Monkhorst-Pack sampling of k -space,²¹ with Gaussian smearing of 0.05 Ry. For the calculation of the DOS we used the tetrahedron method²² with a finer k -point mesh of $36 \times 36 \times 1$ grid.

The band structures of C_6Li , with unrelaxed carbon atom positions, and C_6^* , i.e., graphene described with the unit cell of C_6Li , are compared in Fig. 1. We note the fourfold degeneracy of the bands at Γ , at the Fermi level (Dirac or neutrality point), in Fig. 1(a), which is due to the folding of K and K' points of the graphene BZ onto Γ in the BZ for C_6^* structure. We also note the linear dispersion of the energy bands in the neighborhood of the Dirac point. In Fig. 1(b), we see a number of changes that appear in the band structure of C_6Li . Of interest for our study is the gap opening of $E_g = 0.39 \text{ eV}$ at the neutrality point. For the C_6Li with fully relaxed positions, including those of carbon atoms, the gap opening is $E_g = 0.41 \text{ eV}$, and otherwise the band structure is quite similar to the unrelaxed case. This means that the change in C-C bond lengths is responsible for only about 5% of the band gap. We also note the lifting of other degeneracies, at K and along the Γ - K direc-

tion. Other changes that can be readily noted, as a result of lithium adsorption, include the appearance of the parabolic-shaped band of lithium, with its minimum located at Γ , at 0.92 eV above the neutrality point. The lithium band weakly hybridizes with the graphene conduction bands, resulting in some shifts and kinks in the bands of graphene. There is a substantial charge transfer of $\gtrsim 0.2e$ per Li atom from lithium layer to graphene, with every carbon atom receiving the same charge of one-sixth of this value, i.e., $\gtrsim 0.03e$. As a result, the Fermi level is raised by 1.5 eV relative to the neutrality point of graphene. A rigid band model is clearly not a complete description, but it can be used to describe the charge transfer, which is another important aspect of this problem.

III. TIGHT-BINDING MODEL

A. Lattice geometry

The band gap of C_6Li is a consequence of the special relationship between its structure and that of the graphene substrate. The Bravais lattice of C_6Li is hexagonal, as it is for graphene, but with a $\sqrt{3}$ times larger lattice parameter and rotated by 30° , as shown in Fig. 2. It is convenient to describe the base vectors of the hexagonal lattice in a standard way, with the lattice parameter used as unit of length, so for C_6Li we use the coordinate system with its x -axis taken along \mathbf{a}_1 in Fig. 2,

$$\mathbf{a}_1 = (1, 0)a, \quad \mathbf{a}_2 = \left(-\frac{1}{2}, \frac{\sqrt{3}}{2}\right)a, \quad (1)$$

where $a = a_0\sqrt{3}$. [Thus the same base vectors [Eq. (1)] describe graphene, i.e., \mathbf{c}_1 and \mathbf{c}_2 in Fig. 2, with $a = a_0$ and with the x axis taken along \mathbf{c}_1 .] The corresponding reciprocal-lattice vectors of the hexagonal lattice are

$$\mathbf{b}_1 = \left(1, \frac{1}{\sqrt{3}}\right)\frac{2\pi}{a}, \quad \mathbf{b}_2 = \left(0, \frac{2}{\sqrt{3}}\right)\frac{2\pi}{a}. \quad (2)$$

We denote the reciprocal-lattice vectors of graphene, which are also given by Eq. (2) relative to its own system, by $\mathbf{d}_{1,2}$. The two sets of vectors $\mathbf{b}_{1,2}$ and $\mathbf{d}_{1,2}$ are related by a 30° rotation and a $\sqrt{3}$ change in scale, i.e., $|\mathbf{b}| = |\mathbf{d}|/\sqrt{3}$.

As shown in Fig. 2, the K points of graphene are located at

$$K: \frac{1}{3}\mathbf{d}_1 + \frac{1}{3}\mathbf{d}_2 \equiv \mathbf{b}_1, \quad K': -\frac{1}{3}\mathbf{d}_1 + \frac{2}{3}\mathbf{d}_2 \equiv \mathbf{b}_2, \quad (3)$$

i.e., the K points of graphene coincide with reciprocal-lattice points of C_6^* . It also follows from Eq. (3) that the K points of graphene belong to the reciprocal lattice of the (3×3) structure. Evidently, $(n\sqrt{3} \times n\sqrt{3})R30^\circ$ and $(3n \times 3n)$ constructions, with n a positive integer, will also share this property. The existence of this kind

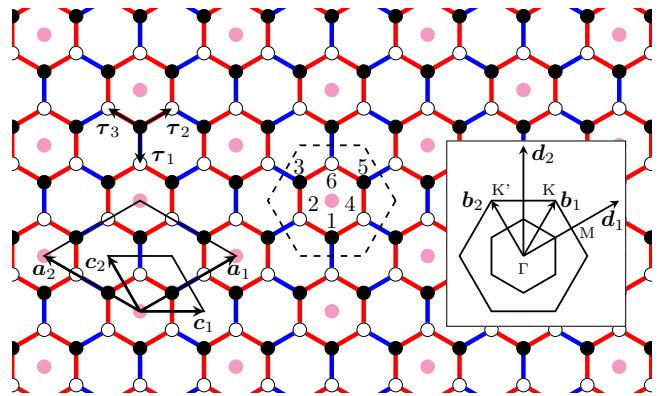


FIG. 2: (Color online) Lattice structure of lithium on graphene C_6Li . Carbon atoms on sublattices A and B are depicted as filled and open black circles. Lithium atoms, in magenta, occupy positions above the hollow sites. The dashed hexagon is the Wigner-Seitz primitive unit cell of C_6Li , containing six numbered C atoms and one Li atom. Two types of bonds, two-thirds red and one-third blue, are distinguished due to the presence of Li atoms. On the lower left, the rhombus defined by \mathbf{c}_1 and \mathbf{c}_2 and enclosing two carbon atoms is the primitive unit cell of graphene. The 30° rotated rhombus, defined by \mathbf{a}_1 and \mathbf{a}_2 and having $\sqrt{3}$ times larger side, is the unit cell of C_6Li . In the upper left part are shown the vectors pointing from a carbon atom on sublattice A to its three nearest neighbors on sublattice B . The inset shows the reciprocal space. The vectors $\mathbf{b}_{1,2}$ and $\mathbf{d}_{1,2}$ are sets of reciprocal lattice vectors of C_6Li and graphene, respectively. The hexagons in the inset are the Brillouin zones. The region defined by ΓKM is the irreducible wedge of graphene Brillouin zone.

of relationship is the basic reason why a gap opens in C_xM if x is a multiple of 3, since in these structures the K points of the underlying graphene become coupled and the perturbation caused by the foreign atoms removes the degeneracy. The wave functions with wave vectors corresponding to K and K' of graphene mix to form different standing waves. One standing wave piles up electronic charge in hexagonal cells occupied by Li, and depletes it from the hexagonal cells devoid of Li, and the other standing wave does the opposite. (The commensurate structure of C_6Li breaks a Z_3 symmetry.) These standing wave states then experience different potentials which qualitatively explains the origin of the gap.

Each carbon atom of sublattice A is connected to three carbon atoms of sublattice B by the $\boldsymbol{\tau}$ vectors, as shown in Fig. 2. These vectors in the coordinate system of C_6Li , needed in our tight-binding calculations, are given by

$$\boldsymbol{\tau}_{1,3} = \left(-\frac{1}{6}, \mp \frac{1}{2\sqrt{3}}\right)a, \quad \boldsymbol{\tau}_2 = \left(\frac{1}{3}, 0\right)a. \quad (4)$$

We now examine the system from the viewpoint of the tight-binding model. The presence of the lithium atoms, in C_6Li , above the hollow hexagonal sites can be imagined to have two effects, within a simple tight-binding model: (a) a contribution (Hartree potential) to the on-site energies of the C atoms, and (b) a possible change in

the hopping amplitudes depicted as C-C bonds in Fig. 2. From an inspection of the Wigner-Seitz cell in Fig. 2, the C atoms are seen to occupy equivalent positions with respect to the metal atoms since each is at a vertex shared by one metal-filled and two empty hexagons of the honeycomb lattice. Therefore all C atoms receive the same charge transfer from Li atoms, as we have also seen in our DFT calculations, and the symmetry breaking cannot be attributed to on-site energies. This reduces the number of parameters and makes a TB model description much simpler for C_6Li than for more dispersed compounds. The bonds, however, occupy two kinds of positions in a Kekulé construction, two-thirds of them (colored red) between a filled and an empty hexagon, and one-third (colored blue) between two empty hexagons. We conclude that there are two different hopping amplitudes corresponding to the two kinds of bond positions. Our DFT calculations showed that changes in bond-length account for $\simeq 5\%$ of the energy gap. The modulation in hopping amplitudes, which are matrix elements of the Hamiltonian between carbon $2p_z$ orbitals, is therefore caused mainly by different potential energies and electron concentrations in the regions of red and blue bonds, with a small contribution due to bond-length distortion. Of course, both variations in potential energy and the distortion of bond lengths are caused by the presence of lithium ions, and their effects on the band gap add with each other.

B. TB Hamiltonian

The π bands of graphene are described well by a Hamiltonian of spinless electrons hopping on the honeycomb lattice of graphene,

$$H = \sum_i \epsilon_i c_i^\dagger c_i - \sum_{ij} t_{ij} c_i^\dagger c_j. \quad (5)$$

Here c_i (c_i^\dagger) annihilates (creates) an electron at site i , ϵ_i are on-site energies, which are all equal and therefore can be set to zero, and t_{ij} are the hopping amplitudes.

The nearest-neighbor TB model of graphene has a gapless band structure, but a Kekulé modulation of the hopping amplitudes couples the K and K' points, leading to a mixing of degenerate states and opening of an energy band gap.²³ Following our discussion above, we allow the hopping amplitudes t_{ij} to have two values, t_1 for two-thirds of the bonds on the hexagonal cells beneath a metal atom, and t_2 for the remaining one-third of the bonds. Here we are interested in describing the gap, and therefore we exclude the metal atoms from our TB model, except for their effect on modulating the hopping amplitudes. They can be included in a more general treatment,²⁴ but this is not needed for describing the gap of C_6Li .

For clean graphene $t_1 = t_2 = t$. There are two π bands corresponding to the two-atom basis, and the band

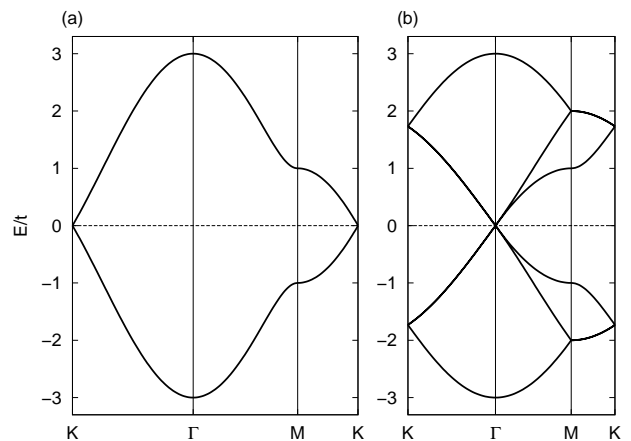


FIG. 3: Band structures of graphene in the Brillouin zones of (a) the (1×1) structure, and (b) the $(\sqrt{3} \times \sqrt{3})R30^\circ$ structure.

energy can be written as

$$E_{\pm}(\mathbf{k}) = \pm t \left| \sum_{i=1}^3 e^{i\mathbf{k} \cdot \boldsymbol{\tau}_i} \right|, \quad (6)$$

where the vectors $\boldsymbol{\tau}_i$ are defined in Fig. 2. When we use the unit cell of the $(\sqrt{3} \times \sqrt{3})R30^\circ$ superlattice to describe graphene, we will have six π bands since there are six carbon atoms within this unit cell. The additional bands are derived from Eq. (6) as $E_{\pm}(\mathbf{k} - \mathbf{b}_1)$ and $E_{\pm}(\mathbf{k} - \mathbf{b}_2)$, with the vectors $\mathbf{b}_{1,2}$ given by Eq. (2), which result in the folding of K and K' points onto the Γ point of BZ, because of relation (3). The energy bands from these analytic formulas are plotted in Fig. 3. It is seen that some degeneracies are present at the new K points [Fig. 3(b)] as well as along ΓK and MK lines. The linear dispersion near the Dirac point is shown in the Appendix to be $E_{\pm}(\mathbf{k}) = \pm \hbar v_F |\mathbf{k}|$, where, $v_F = \sqrt{3} a_0 t / 2 \hbar$ is the Fermi velocity, t is the nearest-neighbor TB hopping parameter, and a_0 is the graphene lattice parameter.

C. Numerical results

We must verify that the band gap of C_6Li can be described by a textured TB model with two different hopping amplitudes, $t_1 \neq t_2$. In this case, we obtain the band structure by numerical diagonalization of the Hamiltonian [Eq. (5)] in momentum space. The method is described in the Appendix, where we also derive an analytic expression for the energy dispersion in the neighborhood of the gap as

$$E_{\pm} = \pm \left(\hbar^2 v_F^2 \mathbf{k}^2 + \frac{E_g^2}{4} \right)^{1/2}, \quad (7)$$

where

$$E_g = 2|t_2 - t_1| \quad (8)$$

for the textured TB model. The Fermi velocity is given in terms of the TB parameter as before, except that now an average value,

$$t = \frac{2t_1 + t_2}{3}, \quad (9)$$

must be used.

From the slope of the linear dispersion near the neutrality point of Fig. 1(a), we can find the Fermi velocity and then the TB parameter $t = 2.72$ eV, in good agreement with the commonly used range for this parameter.²⁵ From Fig. 2(b), we can find the renormalized Fermi velocity v_F and thus the hopping amplitude t by fitting Eq. (7) to the band-structure data in the vicinity of the gap. We found that the value of t is slightly larger for the upper branch than that for the lower branch, by ~ 0.1 eV, but that the change in the average value is much smaller than this amount. In the following, we neglect the renormalization of the Fermi velocity and the average hopping amplitude.

Given the values of $t = 2.72$ eV and $E_g = 0.39$ eV, from first-principles calculations, we can determine t_1 and t_2 from Eqs. (8) and (9). Thus we find $t_1 = 2.79$ eV and $t_2 = 2.59$ eV. Interchanging t_1 and t_2 is also a solution since E_g depends on the absolute value of their difference. To distinguish between the two, we plot the band structures corresponding to both results in Fig. 4. The band gaps are identical in Figs. 4(a) and 4(b), but a characteristic difference can be seen in the way the threefold degeneracy is lifted at K . Comparing with Fig. 1(b), it is seen that Fig. 4(a) has the same qualitative feature, i.e., the same shape of band gap, and the lifting of degeneracies along ΓK and at the K point. This shows the validity of the Kekulé textured model for describing lithium adsorbed graphene, as well as showing that for C_6Li , $t_1 > t_2$. In fact, Fig. 4(b) corresponds to our DFT calculations of the band structure of C_3Li (not shown), which has the same lattice structure as C_6Li , and is its complement.

A useful quantity that can be calculated from energy bands obtained is the density of states per unit cell given by

$$g(E) = 2A \sum_{n=1}^6 \int_{\text{BZ}} \frac{d\mathbf{k}}{(2\pi)^2} \delta[E - E_n(\mathbf{k})], \quad (10)$$

where A is the area of the C_6^* unit cell. For the TB DOS we used a 60×60 k -point mesh and the triangle method,²⁶ which is the two-dimensional version of the tetrahedron method²² that we also used for the *ab initio* calculations. The density of states calculated by first-principles DFT and our TB model compare favorably in the vicinity of the gap, as shown in Fig. 5. The extra densities of states in the energy range above the gap in Fig. 5(a) are due to the band of the lithium atoms, which are not included in our tight-binding model. The other main difference between the two results is the positions of the Van Hove singularities which are closer to the gap in first principles calculations.

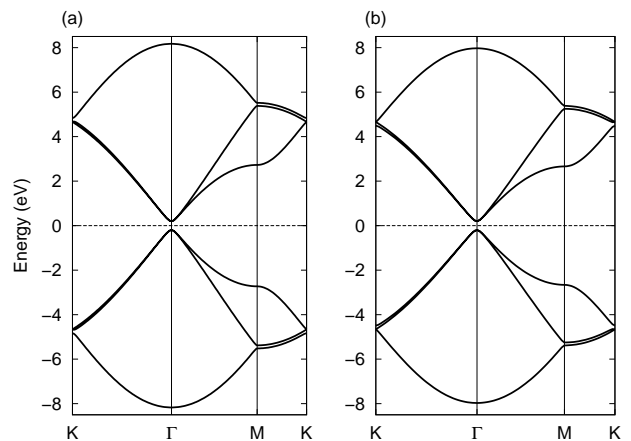


FIG. 4: Band structures of graphene from the TB model with two hopping amplitudes: (a) $t_1 = 2.79$ eV, $t_2 = 2.59$ eV, and (b) $t_1 = 2.59$ eV, $t_2 = 2.79$ eV. Note that the three-fold degeneracies at K , e.g., the lower left one, are lifted so that in (a) we have first a non-degenerate level and above it a doubly degenerate level, and in (b) we have just the opposite order of the degenerate and nondegenerate levels.

IV. SUMMARY

We have studied the opening of a band gap induced in single layer graphene by the adsorption of a submonolayer of an alkali metal. A band gap induced by the adsorption of alkali metals was previously observed in graphite, and its origin was explained to be due to charge transfer to substrate and interlayer interaction of graphene layers. In single layer graphene, where interlayer interaction does not exist, the origin of an alkali-metal induced band gap is in the coupling of K and K' points which is only possible for appropriate superstructures. The required property exists in the superstructures $(3n \times 3n)$ and $(n\sqrt{3} \times n\sqrt{3})R30^\circ$, with n as a positive integer. For other coverages on graphene we expect the bands to remain degenerate at the K points of graphene, resulting in a gapless spectrum. A tight-binding model with alternating hopping amplitudes forming the Kekulé construction was shown to describe the characteristic features of the band structure of C_6Li . From our DFT calculation, we concluded that the modulation of the hopping amplitudes is mainly due to variations in charge density in the graphene plane due to the attraction caused by the Li ions. A tiny distortion of bond lengths additively contributes $\sim 5\%$ to the band gap and, thus, enhances the modulation in hopping amplitudes. In conclusion, we showed that the band gap opening in the lithium on graphene compound C_6Li is consistent with the nearest-neighbor tight-binding model of graphene with Kekulé modulated hopping amplitudes.

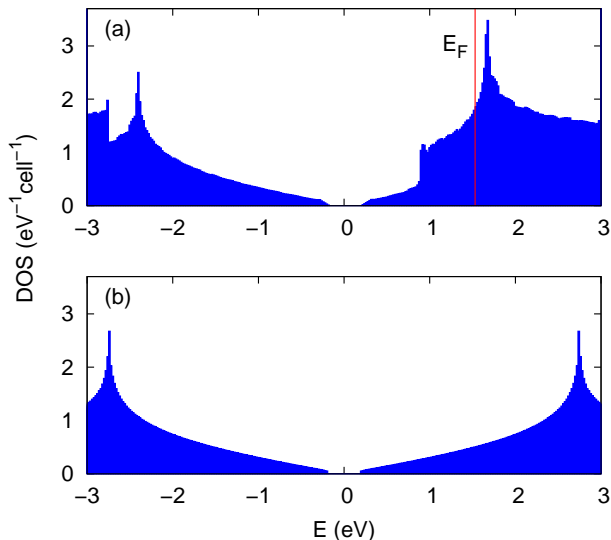


FIG. 5: (Color online) (a) DOS of C_6Li calculated by DFT code. The vertical red line indicates the position of the Fermi level. (b) The corresponding DOS for graphene calculated within the tight-binding model. The position of Van Hove singularities are displaced relative to the DOS of (a) and the extra densities corresponding to Li atoms are not included in (b).

Acknowledgments

M. F. thanks S. Farjam for graphical assistance and A. Saffarzadeh for useful discussions. First principles computations were performed with the resources of the Computational Nanotechnology Supercomputer Centre at the Institute for Research in Fundamental Sciences

(IPM). The financial support of the Iranian Nanotechnology Initiative (INI) is gratefully acknowledged.

APPENDIX: SOLUTION OF TB MODEL

In this appendix, we summarize our method of solving the Kekulé textured nearest-neighbor tight-binding model [Eq. 5]. First, we expand the eigenfunctions of our general periodic system, characterized by crystal momentum \mathbf{k} , in terms of the $2p_z$ orbitals, $|nj\rangle$, localized on the j th atom in the n th unit cell, as

$$|\mathbf{k}\rangle = \frac{1}{\sqrt{N}} \sum_{n=1}^N \sum_{j=1}^M A_j e^{i\mathbf{k}\cdot\mathbf{r}_{nj}} |nj\rangle. \quad (\text{A.1})$$

Here N is the number of unit cells, and M is the number of carbon atoms in the basis, \mathbf{r}_{nj} are position vectors of the atoms, and the amplitudes A_j form the components of the eigenvectors to be determined by diagonalizing the Hamiltonian. For graphene $M = 2$, and the Hamiltonian matrix in momentum space is given by

$$H(\mathbf{k}) = -t \begin{pmatrix} 0 & \sum_{i=1}^3 e^{i\mathbf{k}\cdot\boldsymbol{\tau}_i} \\ \sum_{i=1}^3 e^{-i\mathbf{k}\cdot\boldsymbol{\tau}_i} & 0 \end{pmatrix}, \quad (\text{A.2})$$

which is readily diagonalized to give Eq. (6).

For the textured model, $M = 6$. Referring to Fig. 2 for numbering of the basis atoms, and the $\boldsymbol{\tau}_i$ vectors, we can write the 6×6 Hamiltonian matrix. For example, to obtain the first row we observe that atom 1 has nearest neighbors 2, 4, and 6 (due to periodicity), and is connected to them by $\boldsymbol{\tau}_3$, $\boldsymbol{\tau}_2$, and $\boldsymbol{\tau}_1$, respectively, with hopping amplitudes t_1 , t_1 , and t_2 . Thus we find

$$H(\mathbf{k}) = - \begin{pmatrix} 0 & t_1 e^{i\mathbf{k}\cdot\boldsymbol{\tau}_3} & 0 & t_1 e^{i\mathbf{k}\cdot\boldsymbol{\tau}_2} & 0 & t_2 e^{i\mathbf{k}\cdot\boldsymbol{\tau}_1} \\ t_1 e^{-i\mathbf{k}\cdot\boldsymbol{\tau}_3} & 0 & t_1 e^{-i\mathbf{k}\cdot\boldsymbol{\tau}_1} & 0 & t_2 e^{-i\mathbf{k}\cdot\boldsymbol{\tau}_2} & 0 \\ 0 & t_1 e^{i\mathbf{k}\cdot\boldsymbol{\tau}_1} & 0 & t_2 e^{i\mathbf{k}\cdot\boldsymbol{\tau}_3} & 0 & t_1 e^{i\mathbf{k}\cdot\boldsymbol{\tau}_2} \\ t_1 e^{-i\mathbf{k}\cdot\boldsymbol{\tau}_2} & 0 & t_2 e^{-i\mathbf{k}\cdot\boldsymbol{\tau}_3} & 0 & t_1 e^{-i\mathbf{k}\cdot\boldsymbol{\tau}_1} & 0 \\ 0 & t_2 e^{i\mathbf{k}\cdot\boldsymbol{\tau}_2} & 0 & t_1 e^{i\mathbf{k}\cdot\boldsymbol{\tau}_1} & 0 & t_1 e^{i\mathbf{k}\cdot\boldsymbol{\tau}_3} \\ t_2 e^{-i\mathbf{k}\cdot\boldsymbol{\tau}_1} & 0 & t_1 e^{-i\mathbf{k}\cdot\boldsymbol{\tau}_2} & 0 & t_1 e^{-i\mathbf{k}\cdot\boldsymbol{\tau}_3} & 0 \end{pmatrix}. \quad (\text{A.3})$$

For general $\mathbf{k} \in \text{BZ}$, we diagonalize Eq. (A.3) numerically, but we obtain an analytic expression for the neighborhood of the gap using perturbation theory.

At $\mathbf{k} = 0$, the unperturbed Hamiltonian, case of $t_1 = t_2 = t$, has four of its eigenvalues equal to 0, with the other two being $\pm 3t$. The corresponding eigenvectors are easily written down by noting that they are related to the K , K' , and Γ points of graphene described by its primitive unit cell,

$$\frac{1}{\sqrt{3}} \begin{pmatrix} 1 \\ 0 \\ \omega \\ 0 \\ \omega^* \\ 0 \end{pmatrix}, \quad \frac{1}{\sqrt{3}} \begin{pmatrix} 0 \\ \omega \\ 0 \\ \omega^* \\ 0 \\ 1 \end{pmatrix}, \quad \frac{1}{\sqrt{3}} \begin{pmatrix} 0 \\ \omega^* \\ 0 \\ \omega \\ 0 \\ 1 \end{pmatrix}, \quad \frac{1}{\sqrt{3}} \begin{pmatrix} 1 \\ 0 \\ \omega^* \\ 0 \\ \omega \\ 0 \end{pmatrix}, \quad \frac{1}{\sqrt{6}} \begin{pmatrix} 1 \\ \pm 1 \\ 1 \\ \pm 1 \\ 1 \\ \pm 1 \end{pmatrix}, \quad (\text{A.4})$$

where $\omega = e^{i2\pi/3}$.

Next we calculate the Hamiltonian matrix in the fourfold degenerate subspace of the zero eigenvalue, spanned by the first four vectors of Eq. (A.4), and expand the result near $\mathbf{k} = 0$ to obtain (cf. Ref. 23)

$$\mathcal{H}(\mathbf{k}) = \begin{pmatrix} 0 & \hbar v_F(k_x - ik_y) & t_2 - t_1 & 0 \\ \hbar v_F(k_x + ik_y) & 0 & 0 & t_2 - t_1 \\ t_2 - t_1 & 0 & 0 & -\hbar v_F(k_x - ik_y) \\ 0 & t_2 - t_1 & -\hbar v_F(k_x + ik_y) & 0 \end{pmatrix}, \quad (\text{A.5})$$

where $v_F = \sqrt{3}a_0t/2\hbar$ as for unperturbed graphene, but with $t = (2t_1 + t_2)/3$. Diagonalizing Eq. (A.5), we find Eq. (7).

-
- ¹ K. S. Novoselov, A. K. Geim, S. V. Morozov, D. Jiang, Y. Zhang, S. V. Dubonos, I. V. Grigorieva, and A. A. Firsov, *Science* **306**, 666 (2004).
- ² K. S. Novoselov, A. K. Geim, S. V. Morozov, D. Jiang, M. I. Katsnelson, I. V. Grigorieva, S. V. Dubonos, and A. A. Firsov, *Nature* **438**, 197 (2005).
- ³ Y. Zhang, Y.-W. Tan, H. L. Stormer, and P. Kim, *Nature* **438**, 201 (2005).
- ⁴ P. Avouris, Z. Chen, and V. Perebeinos, *Nat. Nanotechnol.* **2**, 605 (2007).
- ⁵ M. Y. Han, B. Özyilmaz, Y. Zhang, and P. Kim, *Phys. Rev. Lett.* **98**, 206805 (2007).
- ⁶ E. McCann, *Phys. Rev. B* **74**, 161403(R) (2006).
- ⁷ S. Y. Zhou, G.-H. Gweon, A. V. Fedorov, P. N. First, W. A. de Heer, D.-H. Lee, F. Guinea, A. H. Castro Neto, and A. Lanzara, *Nature Mater.* **6**, 770 (2007).
- ⁸ A. Grüneis and D. V. Vyalikh, *Phys. Rev. B* **77**, 193401 (2008).
- ⁹ G. Giovannetti, P. A. Khomyakov, G. Brocks, P. J. Kelly, and J. van den Brink, *Phys. Rev. B* **76**, 073103 (2007).
- ¹⁰ B. Uchoa, C.-Y. Lin, and A. H. Castro Neto, *Phys. Rev. B* **77**, 035420 (2008).
- ¹¹ G. Giovannetti, P. A. Khomyakov, G. Brocks, V. M. Karpan, J. van den Brink, and P. J. Kelly, *Phys. Rev. Lett.* **101**, 026803 (2008).
- ¹² M. Caragiu and S. Finberg, *J. Phys.: Condens. Matter* **17**, R995 (2005).
- ¹³ M. Pivetta, F. Patthey, I. Barke, H. Hövel, B. Delley, and W.-D. Schneider, *Phys. Rev. B* **71**, 165430 (2005).
- ¹⁴ K. Rytkönen, J. Akola, and M. Manninen, *Phys. Rev. B* **75**, 075401 (2007).
- ¹⁵ K. T. Chan, J. B. Neaton, and M. L. Cohen, *Phys. Rev. B* **77**, 235430 (2008).
- ¹⁶ M. Calandra and F. Mauri, *Phys. Rev. Lett.* **95**, 237002 (2005).
- ¹⁷ M. Calandra and F. Mauri, *Phys. Rev. B* **76**, 161406(R) (2007).
- ¹⁸ P. Giannozzi *et al.*, <http://www.quantum-espresso.org>; we used the norm-conserving pseudopotentials C.pz-vbc.UPF and Li.pz-n-vbc.UPF from this distribution.
- ¹⁹ J. P. Perdew and A. Zunger, *Phys. Rev. B* **23**, 5048 (1981).
- ²⁰ D. M. Ceperley and B. J. Alder, *Phys. Rev. Lett.* **45**, 566 (1980).
- ²¹ H. J. Monkhorst and J. D. Pack, *Phys. Rev. B* **13**, 5188 (1976).
- ²² P. E. Blöchl, O. Jepsen, and O. K. Andersen, *Phys. Rev. B* **49**, 16223 (1994).
- ²³ C.-Y. Hou, C. Chamon, and C. Mudry, *Phys. Rev. Lett.* **98**, 186809 (2007).
- ²⁴ H. Ishida and R. E. Palmer, *Phys. Rev. B* **46**, 15484 (1992).
- ²⁵ S. Reich, J. Maultzsch, C. Thomsen, and P. Ordejón, *Phys. Rev. B* **66**, 035412 (2002).
- ²⁶ J.-H. Lee, T. Shishidou, and A. J. Freeman, *Phys. Rev. B* **66**, 233102 (2002).